RSC Advances

ROYAL SOCIETY OF CHEMISTRY

www.rsc.org/advances

Table of contents entry

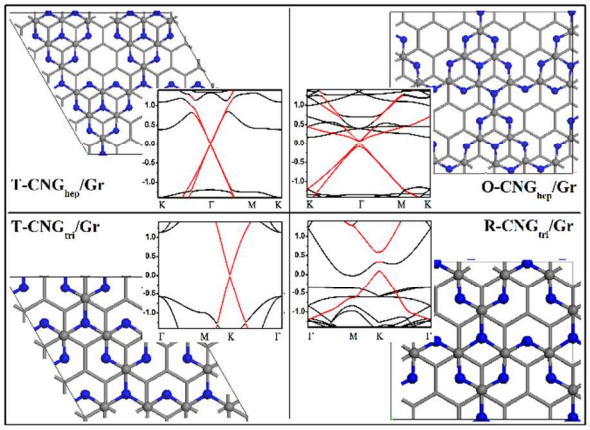

Due to the nonequivalent sub-lattices and interface hybridization, size and symmetry-dependent band gap opens in graphene induced by g-C_3N_4 substrates.

Nanoscale

RSCPublishing

ARTICLE

Symmetry-dependent band gap opening in graphene induced by g-C_3N_4 substrates

Cite this: DOI: 10.1039/x0xx00000x

Ji-Chang Ren[a,b,c], Rui-Qin Zhang[b], Zejun Ding[a] and Michel A. Van Hove[d]

Received ooth January 2012,
Accepted ooth January 2012

DOI: 10.1039/x0xx00000x

www.rsc.org/

Opening the band gap in graphene can significantly broaden its applications in electronic devices. By introducing four types of graphene-like carbon nitride (g-C_3N_4) as the substrate of graphene, we reveal, with first principles calculations, symmetry and size dependent band gap opening in graphene. On the one hand, for a substrate with a 3-fold rotational symmetry, a small C_3N_4 unit can cause a large value of the band gap in the graphene layer. On the other hand, the band gap also depends on the symmetry of the substrate. A 3-fold symmetry induces a relatively small band gap, while rectangular and oblique symmetries result in a relatively large band gap opening in graphene but cause a much heavier effective mass of charge carriers. The former case is due to the nonequivalence of sub-lattices in graphene induced by the substrate, while for the latter case, interfacial hybridization plays the main role in band gap opening in graphene. Our theoretical findings can pave the way for the use of graphene-based semiconductor devices.

Introduction

Due to its high carrier mobility, graphene has been considered to be one of the most likely candidates for the development of the next generation of nano-devices. However, the intrinsic zero band gap of graphene obstructs its further applications in field effect transistors (FETs). Thus, opening and tuning the band gap of graphene has been one of the important issues in the applications of graphene-based nano-devices. Many methods have been proposed to open the band gap in graphene. Generally, they can be classified into three types: 1. size effect[1,2]; 2. destroying the symmetry of graphene by introducing an antidote lattice[3], chemical functionalization[4-6], inhomogeneous strain[7], or substituting carbon atoms with foreign atoms[8,9]; and 3. substrate effect[10-13]. The first two methods can induce a relatively large gap opening, but cause significant reduction of the carrier mobility due to the scattering centres arising from the boundaries, defects or substituted sites.

Different from the first two methods, the third approach has the following advantages: first, the required epitaxial graphene layers can be synthesized and controlled much more easily than can doping and chemical functionalization in graphene; second, due to the weak Van der Waals interactions with substrates, the π electrons in graphene are only weakly modified, retaining most characteristics of a Dirac cone; third, the band gap can be tuned by changing the interactions between substrates and graphene through controlling the interlayer distance[14] or perpendicular electric field[15].

Experimentally, the epitaxial graphene layers are fabricated mostly on SiO_2[16] or SiC[17]. However, due to their rough surfaces and lattice mismatch, high-quality graphene sheets are hard to obtain[18]. Recently, the successful synthesis of high-quality graphene on hexagonal boron nitride[19,20] has paved the way for the substrate-based electronic tailoring of graphene. Another hexagonal layered structure is graphitic carbon nitride (g-C_3N_4), which has been proposed as an excellent photocatalyst. Using g-C_3N_4 as a substrate of graphene[21], not only can the band gap be opened in graphene but also the photocatalytic activity in the visible light range for the g-C_3N_4 substrate can be clearly enhanced. In experiments, the graphene-g-C_3N_4 hetero-structure has been successfully synthesized[22], which extends the possibility of the electronic engineering of graphene.

[a]*Department of Physics, University of Science and Technology of China,Hefei, China. E-mail: zjding@ustc.edu.cn;*
[b]*Department of Physics and Materials Science, City University of Hong Kong, Hong Kong SAR, China. E-mail: aprqz@cityu.edu.hk;*
[c]*USTC-CityU Joint Advanced Research Centre, Suzhou, 215123, China*
[d]*Institute of Computational and Theoretical Studies & Department of Physics, Hong Kong Baptist University, Hong Kong SAR, China. E-mail:vanhove@hkbu.edu.hk*

The possible origin of the substrate induced band gap opening in graphene has been attributed to the lifting of the equivalence of its two carbon sub-lattices. More specifically, due to the electrostatic potential difference[14] (EPD) induced by the substrate, charge redistribution occurs in the graphene. Therefore, by tuning the EPD, the band gap in graphene can easily be controlled. Numerical calculations[23] show that periodically patterned gates on graphene can induce band gap opening. As a result, the super-lattice with different symmetry in graphene results in band gap opening. However, these patterned gates are difficult to produce experimentally at the nano-scale. So far, most of the studies based on first principles calculations have focused on the stacking order or different strengths of EPD induced by substrates; the symmetry effect induced by the substrate has been seldom investigated.

In this work, we investigate the band gap opening in a graphene layer tuned by a g-C_3N_4 single layer substrate. Using four types of single layer g-C_3N_4 substrates with different symmetries as well as different sizes of the C_3N_4 unit, we revealed that the interactions between substrate and graphene can be significantly altered. For the substrates with 3-fold rotational symmetry, smaller C_3N_4 units can induce larger band gaps in graphene; for substrates with non-3-fold symmetry, more deviation from 3-fold symmetry will induce larger modification of the Dirac cones, and result in larger band gap opening in the graphene.

The EPD effect has been proposed as the main origin of the band gap opening in graphene induced by a single-layer substrate. In the case of boron nitride (BN) on graphene (Gr), due to the weak interlayer interaction, little orbital hybridization occurs at the interface between layers, resulting in slight band gap opening. In this work, by introducing g- C_3N_4 substrates with different geometric structures, we found that the interfacial hybridization is enhanced by tuning the symmetry of the substrate. Therefore, the band gap becomes larger in graphene but at the cost of lowering the effective mass at the Dirac point. Our results provide a way to tune the band structure of Dirac cones, which can be significantly important in the applications of electronic nano-devices.

Geometrically, g-C_3N_4 is composed of triazine[24] units or heptazine[25] units. Both C_3N_4 units show triangular shape but the size of the unit is larger for heptazine. With different sizes of C_3N_4 units and connection patterns, four types of g-C_3N_4 allotropes are formed, which are denoted as CNG substrates, as shown by balls and sticks in Fig. 1 . Two of them show 3-fold symmetry but with different C_3N_4 units, which are denoted as T-CNG_{tri} and T-CNG_{hep}; the symmetries of the other two allotropes are rectangular (R) and oblique (O) respectively, and these two are denoted as R-CNG_{tri} and O-CNG_{hep}, respectively. The stabilities of the four allotropes have been discussed previously[26-28]. Since the main purpose in this paper is to study the symmetry effect on the modification of Dirac cones in graphene, the formation energies of the systems as well as the relative stabilities between them will not be discussed here.

Computational details

To relax the CNG/Gr bilayer systems, first principles calculations were performed with the SIESTA-trunk package[29]. The double zeta (DZP) basis set was chosen with an energy shift of 10 meV. Norm-conserving pseudo-potentials[30] were used to describe the interactions between the core ions and valence electrons. VdW-DF1 long-range dispersion functionals[31] were applied to describe the Van der Waals interaction between layers. The Brillouin zone summations were carried out with the Monkhorst-Pack scheme. We applied 6×6×1 Monkhorst-Pack k-points for the structure relaxation, while for electronic property calculations, the Brillouin zone was sampled using 16×16×1 k-points. A dipole correction was applied to subtract the artificial dipole moment between periodic cells. The vacuum perpendicular to the bilayer was set to no less than 18 Å, which is large enough to ignore the interactions between cells.

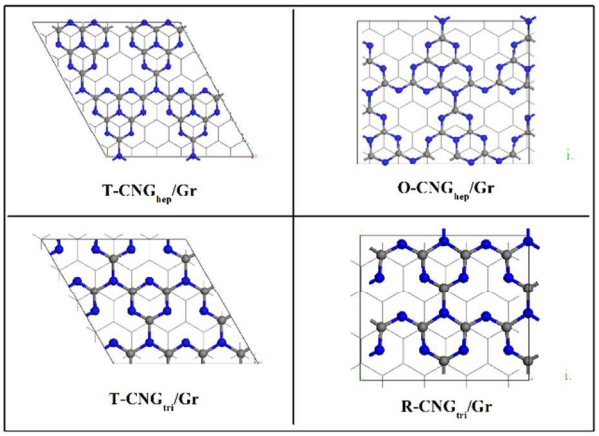

Fig.1 Geometric structures of CNG/Gr bilayer systems. The graphene layer is indicated by gray lines; CNG substrates are represented by balls and sticks, where nitrogen and carbon atoms are shown as blue and grey spheres, respectively. All four bilayer systems have AB-stacking. The substrates are named T-CNG_{hep}, O-CNG_{hep}, T-CNG_{tri} and R-CNG_{tri}, where the first letter of the names represent their symmetries: 3-fold or triangular (T), oblique (O), rectangular (R), while the subscripts represent the C_3N_4 unit: heptazine (hep) and triazine (tri).

Results and discussion

The optimized geometric structures are shown in Fig. 1. All four types of substrate were slightly buckled due to the repulsion between the lone pair electrons on the two-coordinated nitrogen atoms. The average interlayer distances were obtained between the centres of the g-C_3N_4 substrate and graphene layer.

Table 1 Band gaps, charge transfers from graphene to CNG substrates, interlayer distances and effective masses of carriers (electrons m_e^* and holes m_h^*) at the Dirac point of several hetero-bilayer systems.

Hetero-bilayer	Band gap (meV)	Charge transfer (electron/atom)	Interlayer distance (Å)	m_h^* (m_e)	m_e^* (m_e)
T-CNG_{hep}/Gr	50.3	0.002	3.15	0.0071 (Γ->K) 0.0065 (Γ->M)	0.0072 (Γ->K) 0.0067 (Γ->M)
O-CNG_{hep}/Gr	69.1	0.006	3.28	0.0102 (0.0065) (Γ->K) 0.0102 (0.0070) (Γ->M)	0.0168 (0.0062) (Γ->K) 0.0136 (0.0072) (Γ->M)
T-CNG_{tri}/Gr	52.3	0.006	3.18	0.0030 (M←K→Γ)	0.0034 (M←K→Γ)
R-CNG_{tri}/Gr	455.7*	0.009	3.20	0.0218 (K->M) 0.0275 (K->Γ)	0.0171 (K->M) 0.0155 (K->Γ)

*Note: a flat band is located in the middle of this band gap.

As shown in Table 1, all the bilayer systems show the interlayer distance as being clearly shorter than that of bilayer graphene as well as that of the BN/Gr bilayer system[14], indicating much stronger interlayer interactions. Due to the interactions between layers, a band gap opens at the Dirac point. Specifically, for the CNG substrate with 3-fold symmetry, the one with larger C_3N_4 units (T-CNG_{hep}) induces larger band gaps in graphene; for the CNG substrate derived from 3-fold symmetry, the induced band gap will become larger. In particular, for the R-CNG_{tri} substrate, the band gap becomes as large as ~455 meV, indicating a much larger interlayer interaction. It should be noted that the band gap of T-CNG_{hep}/Gr is 70 meV in Ref. (21), slightly larger than our result here (~50 meV). This is because the interlayer distance is about 0.15 Å larger than their result due to the different VdW scheme used. Since the mechanism of band gap opening is not dependent on the VdW scheme used, we do not discuss this aspect in this paper.

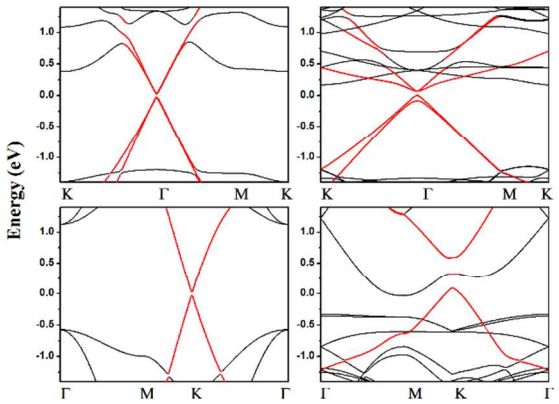

Fig. 2 Band structures of CNG/Gr bilayer systems. The red lines indicate the modified Dirac cone in graphene. The Fermi level is set to zero.

To further analyze the modification of the Dirac cone in graphene, we calculated the band structures of the hetero-bilayer systems. As shown in Fig. 2, for CNG substrates with heptazine units, the modified Dirac cone in graphene appears at the Γ special point while for the ones with triazine units, it remains at the special point K. For the CNG substrate with 3-fold symmetry, the Dirac cone in graphene is slightly modified and the linear dispersion around the Dirac point is almost maintained. However, when the substrate deviates from 3-fold symmetry, the modification of the Dirac cone becomes obvious: first, the band gaps in graphene clearly increase; second, the slopes of the conduction bands and valance bands decrease, indicating much lower carrier mobility. To evaluate the carrier mobility, we also calculated the effective mass of electron and hole carriers at the Dirac point based on the expression $m^* = \frac{\hbar^2 dk^2}{d^2E}$. As shown in Table 1, massless and almost massless carriers exist in the T-CNG_{tri}/Gr and T-CNG_{hep}/Gr systems, respectively, while relatively heavy carriers exist in the R-CNG_{tri}/Gr and O-CNG_{hep}/Gr systems, indicating stronger interaction between layers for the latter cases.

In previous studies, band gap opening was explained as being due to charge redistribution in the graphene layer, which causes the inequivalent sub-lattices in graphene. Little orbital overlap between graphene and substrate layers was observed. However, in the cases studied here, considering the obvious modification of Dirac cones in the R-CNG_{tri}/Gr and O-CNG_{hep}/Gr systems, it seems that other factors may also have important impacts on the band gap in graphene.

In order to understand the origin of band gap opening, the electron coupling between graphene and CNG substrates was analyzed by characterizing the charge density difference. These differences were obtained by subtracting the electronic charge of hetero-bilayer systems from the charges of independent graphene and CNG substrates, as shown in Fig. 3. Due to the inhomogeneous CNG substrates, π electrons in graphene are redistributed correspondingly. As a result, electron and hole puddles are formed with different sizes and patterns. The previous studies only considered charge redistribution with 3-fold symmetry due to the substrate used. In this study, since four types of CNG substrates have been introduced, it is possible to study the symmetry as well as the size effect on the band gap opening.

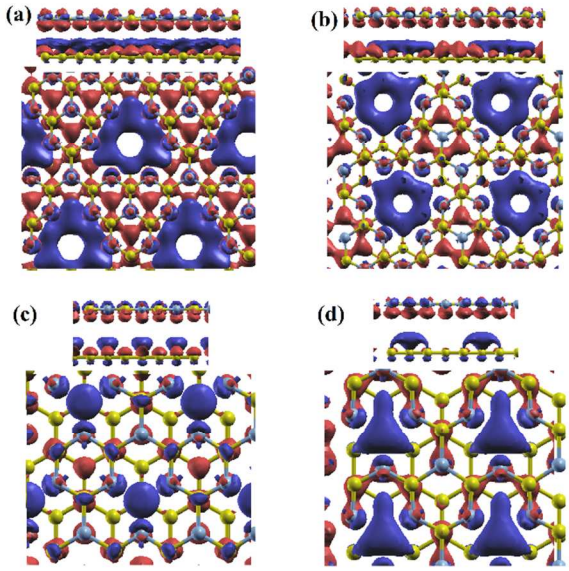

Fig. 3 Top and side views of the differential charge distribution of CNG/Gr bilayer systems. Yellow and light blue balls represent carbon and nitrogen atoms, respectively. Red and blue isosurfaces represent, respectively, charge accumulation and depletion in real space with respect to isolated graphene and the CNG substrate.

The T-CNG_{hep} and T-CNG_{tri} substrates have the same symmetry but possess different sizes of C_3N_4 units. Due to the EPD effect, the symmetry of graphene is reduced from 6-fold to 3-fold rotational symmetry but with different sizes of electron and hole puddles, as shown in Fig. 3 (a) and (c). The smaller size of electron and hole puddles induces larger band gap opening. On the other hand, a smaller C_3N_4 unit results in larger charge transfer from the graphene to the CNG substrate, indicating stronger interfacial electron coupling, which further increases the band gap in graphene. When a T-CNG_{hep} (resp. T-CNG_{tri}) substrate is replaced by O-CNG_{hep} (R-CNG_{tri}), the symmetry of graphene changes to oblique (rectangular). At the same time, the corresponding charge transfer from the graphene to the CNG substrate increases, indicating larger orbital overlap between graphene and substrate. Comparing O-CNG_{hep}/Gr and T-CNG_{tri}/Gr, it is found that, in both bilayer systems, the same amount of charge is transferred from graphene to CNG substrates. However, in O-CNG_{hep}/Gr, a larger band gap opens

in the graphene, although the interlayer distance is about ~0.1Å larger than that in the T-CNG$_{tri}$/Gr bilayer. This indicates that the symmetry of O-CNG$_{hep}$/Gr plays a role in the band gap opening.

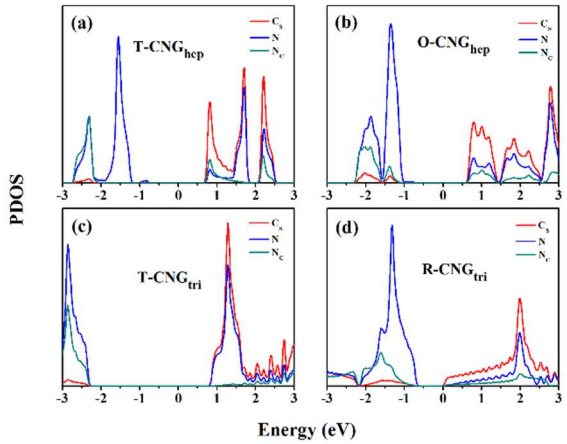

Fig. 4 Partial density of states (PDOS) of four different single-layer CNG substrates. C_S represents the carbon atoms. N and N_C represent, respectively, the two-coordinated and three-coordinated nitrogen atoms. Red, blue and dark cyan lines indicate, respectively, the density of states of the C_S, N and N_C atoms. The Fermi energy is set to zero.

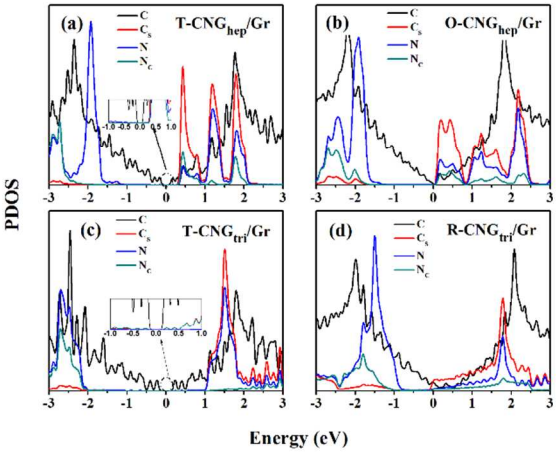

Fig. 5 Partial density of states (PDOS) of CNG/Gr bilayer systems. C and CS represent, respectively, the carbon atoms of graphene and the CNG substrate, and N and N_C represent, respectively, the two-coordinated and three-coordinated nitrogen atoms of the CNG substrate. Black, red, blue and dark cyan lines indicate, respectively, the density of states of C, C_S, N and N_C atoms. The Fermi energy is set to zero. The insets in (a) and (c) are the enlarged PDOS close to Fermi level.

To further understand the symmetry effect of the substrates, as a comparison, we firstly calculated the partial density of states (PDOS) of single-layer CNG substrates, as shown in Fig. 4. The frontier orbitals are almost the same for the four types of CNG substrates: the Highest Occupied Molecular Orbital (HOMO) arises from the two-coordinated nitrogen atoms and the Lowest Unoccupied Molecular Orbital (LUMO) is mainly contributed from the p_z orbital of carbon atoms. However, their band gaps are totally different. Although the GGA approximation cannot accurately evaluate the exact value of the band gaps of CNG substrates, it is reasonable to compare these gaps. As shown in Table 1, they exhibit the trend: T-CNG$_{tri}$ > T-CNG$_{hep}$ > O-CNG$_{hep}$ > R-CNG$_{tri}$. Thus, when the symmetry of the CNG substrate deviates from triangular symmetry, the band gap decreases. In particular, from triangular symmetry to rectangular symmetry, the band gap decreases from 3.19 to 0.75 eV, as shown in Fig. 4 (c) and (d).

In order to investigate the hybridization effect at the interface, the PDOS of the hetero-bilayer systems were also calculated. As seen in Fig. 5, due to the electron coupling at the interface, for all four substrates, the LUMO shifts down close to the Fermi level. Especially for R-CNG$_{tri}$/Gr, its LUMO moves slightly below the Fermi level, indicating a semiconductor—metal transition. However, the hybridization effect between the π electrons in graphene and CNG substrates is different: for substrates with triangular symmetry, the hybridization at the interface can be ignored, as shown in Fig. 5 (a) and (c), while for substrates with non-triangular symmetry, as in Fig. 5 (b) and (c), distinct hybridization occurs between the π electrons at the interface. Interestingly, although the amount of charge transfer from the graphene to the O-CNG$_{hep}$ and T-CNG$_{tri}$ substrates is the same, the orbital overlap at the interface is much larger in the O-CNG$_{hep}$/Gr system (almost no hybridization exists in the T-CNG$_{tri}$/Gr system). This can be partially explained by their chemical potential difference with graphene, which can be simply estimated from their band gaps. Graphene is a gapless semi-metal, and O-CNG$_{hep}$ has a much smaller band gap than T-CNG$_{tri}$. Thus, the π electrons in graphene prefer to couple with the π electrons in O-CNG$_{hep}$. The largest hybridization occurs for the R-CNG$_{tri}$ substrate, since its chemical potential is very close to that of graphene. On the other hand, the triangular symmetry in graphene only destroys the equivalence of the sub-lattices but maintains the symmetry of the sub-lattice, while the non-triangular symmetry in graphene induces the loss of equivalence as well as the symmetry of the sub-lattices.

Thus, both the hybridization and the symmetry affect the band gap opening in graphene. When the symmetry of the CNG substrate deviates from triangular, the band gap in graphene becomes larger. However, the modification of the Dirac cone increases at the same time. Thus, the calculated effective masses for graphene with the O-CNG$_{hep}$ and R-CNG$_{tri}$ substrates are much larger than those with the T-CNG$_{hep}$ and T-CNG$_{tri}$ substrates. Furthermore, for the R-CNG$_{tri}$ substrate, a flat band appears in the gap of graphene.

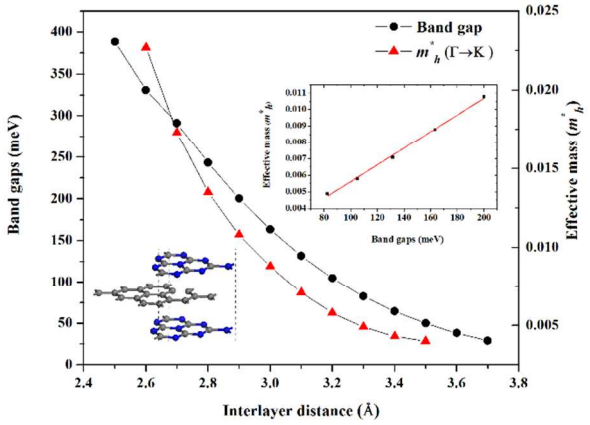

Fig. 6 Values of the band gap and the effective mass of carriers as a function of interlayer distance. The left insert shows the geometric structure of a sandwich structure of T-CNG$_{hep}$/Gr/T-CNG$_{hep}$ tri-layer systems with ABA stacking. The right insert shows the relationship of the band gap with the effective mass of hole carriers at the Dirac point.

By comparing the system with the T-CNG$_{hep}$ and O-CNG$_{hep}$ substrates, it is evident that the band gap can be tuned by

changing the symmetry of the substrate. Since T-CNG_{hep} and O-CNG_{hep} have almost the same band gaps, indicating similar chemical potential differences with graphene, a chemical potential difference induced interfacial hybridization should have a similar effect. However, a relatively larger band gap opens in graphene for the system with the O-CNG_{hep} substrate. In Table 1, it can be seen that although the interlayer distance is larger in O-CNG_{hep}/Gr than in T-CNG_{hep}/Gr, the charge transfer is larger for O-CNG_{hep}/Gr than for T-CNGhep/Gr. For single-layer graphene, it is known that the π electronic structure displays very high rigidity. However, in the case of O-CNG_{hep}/Gr, due to the breaking of the symmetry of the sub-lattices, the rigidity of π conjugation can be significantly reduced. Therefore, larger charge transfer occurs for O-CNG_{hep}/Gr than for T-CNG_{hep}/Gr.

Since no or little hybridization appears at the interface between graphene and the CNG substrate with triangular symmetry, the linear dispersion is retained (or changed little). Thus, substrates with triangular symmetry show superiority over ones with non-triangular symmetry in the applications of semi-conductor devices with super high carrier mobility. For potential applications, we designed a sandwich structure with ABA stacking as shown in the inset in Fig. 6. It is found that the value of the band gap in graphene is ~133 meV, which is almost twice that of the bilayer system discussed in Ref. (21). To evaluate the distance effect between layers, we calculated the band gaps and the effective mass of the hole carriers for decreasing interlayer distances. As shown in Fig. 6, a linear relationship exists between the band gap and effective mass, which is consistent with the previous expression to describe Dirac fermions based on the π-electron tight-binding model: $|M^*| \approx E_g/2v_F^2$, where v_F is Fermi velocity. The calculated v_F is almost 10^6 m/s, which is higher than the one modulated by a BN substrate (0.8×10^6 m/s)[32].

Conclusions

In summary, based on first principles calculations, four types of single-layer CNG substrates were investigated to tune the π-electronic structure in graphene. It was found that the band gap in graphene is dependent on the symmetry of the substrate as well as the size of the C_3N_4 unit. A smaller C_3N_4 unit induces a larger band gap opening in graphene. For CNG substrates with 3-fold rotational symmetry, the band gap opens at the Dirac point with relatively small values, but the mobility of charge carriers is higher than the one caused by BN substrate. For the CNG substrates deviating from 3-fold rotational symmetry, a relatively large band gap opens in graphene. The band gap opening in the four cases is attributed to the electrostatic potential difference (EPD) as well as the interfacial hybridization. For substrates with 3-fold rotational symmetry, the EPD effect plays the main role in the band gap opening, while for substrates deviating from 3-fold rotational symmetry both the EPD and interfacial hybridization impact the band gap opening in graphene. On the one hand, the smaller chemical potential difference between graphene and substrate induces larger interfacial hybridization; on the other hand, the rigidity of π conjugation in graphene can be reduced more effectively by a substrate with non-3-fold rational symmetry, which further enhances the interfacial hybridization. For applications in electronic devices with high carrier mobility, we propose a sandwich structure which can increase the band gap opening in graphene without destroying the linear dispersion of the Dirac cone. Our finding provides a deeper understanding of the symmetry effect on the band gap opening in graphene induced by the substrate. Through tuning the band structure of the Dirac cone in graphene by using substrates with different symmetries, the applications of graphene in electronic devices can be further extended.

Acknowledgements

The work described in this paper is supported by a grant from the Research Grants Council of Hong Kong SAR [Project No. CityU 103913] and the Centre for Functional Photonics (CFP). MAVH was supported by the HKBU Strategic Development Fund. We thank the High Performance Cluster Computing Centre, Hong Kong Baptist University, which receives funding from the Research Grants Council, University Grants Committee of the HKSAR and Hong Kong Baptist University.

References

1 R. Q. Zhang, E. Bertran, S. -T. Lee, *Diam. Relat. Mater*., 1998, **7**, 1663-1668.
2 Y.-W. Son, M. L. Cohen and S. G. Louie, *Phys. Rev. Lett*., 2006, **97**, 216803.
3 T. G. Pedersen, C. Flindt, J. Pedersen, N. A. Mortensen, A. -P. Jauho, and K. Pedersen, *Phys. Rev. Lett*., 2008, **100**, 136804.
4 R. Balog, B. Jørgensen, L. Nilsson, M. Andersen, E. Rienks, M. Bianchi, M. Fanetti, E. Lægsgaard, A. Baraldi, S. Lizzit, Z. Sljivancanin, F. Besenbacher, B. Hammer, T. G Pedersen, P. Hofmann and L. Hornekær, *Nat. Mater*., 2010, **9**, 315-319.
5 F.Withers, M. Dubois and A. K. Savchenko, *Phys. Rev. B*, 2010, **82**, 073403.
6 M. Mirzadeh and M. Farjam, *J. Phys.: Condens. Matter*., 2012, **24**, 235304.
7 I. I. Naumov and A. M. Bratkovsky, *Phys. Rev. B*, 2011, **84**, 245444.
8 D. Usachov, O. Vilkov, A. Grueneis, D. Haberer, A. Fedorov, V. K. Adamchuk, A. B. Preobrajenski, P. Dudin, A. Barinov, M. Oehzelt, *Nano Lett*., 2011, **11**, 5401-5407.
9 A. K. Manna and S. K. Pati, *J. Phys. Chem. C*, 2011, **115**, 10842-10850.
10 S. Y. Zhou, G.-H. Gweon, A. V. Fedorov, P. N. First, W. A. de Heer, D.-H. Lee, F. Guinea, A. H. Castro Neto and A. Lanzara, *Nat. Mater*., 2007, **6**, 770-775.
11 C.-L. Lin, R. Arafune, K. Kawahara, M. Kanno, N. Tsukahara, E. Minamitani, Y. Kim, M. Kawai and N. Takagi, Phys. Rev. Lett., 2013, **110**, 076801.
12 G. Giovannetti, P. A. Khomyakov, G. Brocks, P. J. Kelly, J. van den Brink, *Phys. Rev. B*, 2007, **76**, 073103.
13 A. Ramasubramaniam, D. Naveh and E. Towe, *Nano Lett*., 2011, **11**, 1070-1075.
14 E. Kan, H. Ren, F. Wu, Z. Li, R. Lu, C. Xiao, K. Deng and J. Yang, *J. Phys. Chem. C*, 2012, **116**, 3142-3146.
15 R. Quhe, J. Zheng, G. Luo, Q. Liu, R. Qin, J. Zhou, D. Yu, S. Nagase, W. -N. Mei, Z. Gao and J. Lu, *NPG Asia Materials*, 2012, **4**, e6.
16 N. Cuong, M. Otani and S. Okada, *Phys. Rev. Lett*., 2011, **106**, 106801.

17 Y. M. Lin, C. Dimitrakopoulos, K. A. Jenkins, D. B. Farmer, H. Y. Chiu, A. Grill and Ph. Avouris, *Science*, 2010, **327**, 662.
18 J. -H. Chen, C. Jang, S. Xiao, M. Ishigami and M. S. Fuhrer, *Nat. Nanotech*., 2008, **3**, 206.
19 J. Xue, J. Sanchez-Yamagishi, D. Bulmash, P. Jacquod, A. Deshpande, K. Watanabe, T. Taniguchi, P. Jarillo-Herrero and B. J. LeRoy, *Nat. Mater*., 2011, **10**, 282-285.
20 C. R. Dean, A. F. Young, I. Meric, C. Lee, L. Wang, S. Sorgenfrei, K. Watanabe, T. Taniguchi, P. Kim, K. L. Shepard and J. Hone, *Nat. Nanotech*., 2010, **5**, 722-726.
21 A. -J. Du, S. Sanvito, Z. Li, D. Wang, Y. Jiao, T. Liao, Q. Sun, Y. -H. Ng, Z. -H. Zhu, R. Amal and S. C. Smith, *J. Am. Chem. Soc*., 2012, **134**, 4393-4397.
22 Q. J. Xiang, J. G. Yu and M. Jaroniec, *J. Phys. Chem. C*, 2011, 115, 7355-7363.
23 R. P. Tiwari and D. Stroud, *Phys. Rev. B*, 2009, **79**, 205435.
24 A. Y. Liu and R. M. Wentzcovitch, *Phys. Rev. B*, 1994, **50**, 10362.
25 E. Kroke, M. Schwarz, E. Horath-Bordon, P. Kroll, B. Noll and A. D. Norman, *New J. Chem*., 2002, **26**, 508-512. X. Ma, Y. Lv, J. Xu, Y. Liu, R. Q. Zhang and Y. Zhu, *J. Phys. Chem. C*, 2012, **116** (44), 23485-23493.
26 X. Ma, Y. Lv, J. Xu, Y. Liu, R. Q. Zhang, Y. Zhu, *J. Phys. Chem. C*, 2012, **116** (44), 23485-23493.
27 A. -S. Gerardo, et al., *Angew. Chem. Int. Ed*, 2014, **53**, 7450-7455.
28 I. Alves, G. Demazeau, B. Tanguy, F. Weill, *Solid State Commun*. 1999, **109**, 697-701.
29 J. M. Soler, E. Artacho, J. D. Gale, A. García, J. Junquera, P. Ordejón, D. Sánchez-Portal, *J. Phys.: Condens. Matter*, 2002, **14**, 2745.
30 D. R. Hamann, M. Schlüter and C. Chiang, *Phys. Rev. Lett*., 1979, **43**, 1494.
31 M. Dion, H. Rydberg, E. Schröder, D. C. Langreth, B. I. Lundqvist, *Phys. Rev. Lett*., 2004, **92**, 246401.
32 Y. Fan, M. Zhao, Z. Wang, X. Zhang and H. Zhang, *Appl. Phys. Lett*., 2011, **98**, 083103.

